Ion-electron emission from a cold metal target covered by xenon

1989 J. Phys.: Condens. Matter 1 1353

(http://iopscience.iop.org/0953-8984/1/7/017)

J. Phys.: Condens. Matter 1 (1989) 1353–1363. Printed in the UK

Ion–electron emission from a cold metal target covered by xenon

W Soszka, S Kwaśny, J Budzioch and M Soszka
Institute of Physics, Jagellonian University, Kraków, Poland

Received 1 March 1988, in final form 5 July 1988

Abstract. The energy spectra of electrons induced by xenon ion bombardment of the Fe–Ni alloy target covered by frozen xenon were measured. Three broad maxima superimposed on the background which ranges from zero to a few hundred electron volts were observed. Excluding the first maximum which is a typical maximum of bulk electrons from the metal the yield of electrons shows some angular anisotropy in the region of large detection angles. It is assumed that the emission of these electrons is connected with the creation of the symmetric quasi-molecules $Xe^+ + Xe^0$. The background is associated with direct ionisation of the quasi-molecules during the approach of the collision particles and the structure of the energy spectrum with outer-shell and inner-shell molecular auto-ionisation processes. The presence of the xenon condensed layer on the metal target was tested by energy analysis of the back-scattered neon ions. The xenon peak and the so-called double-scattering maximum which is attributed to the solid state were found on the energy distribution curve.

1. Introduction

Interaction of ions with the solid surface leads to electron emission and a few sources of electrons can be distinguished (Krebs 1968). Most of the experimental studies were carried out on the assumption that the only source of electrons is the target material (Benazeth 1982). Usually, the role of embedded projectiles and adsorbed or contaminant particles as a source of electrons is neglected. Such treatment of the electron emission problem is not correct because, if the measurements have been performed in a differential manner, the presence of such particles is manifested by some structure in the energy and angular distributions (Soszka and Soszka 1983). The surface adsorbed layer essentially determines the features of the ion–electron emission under 'classical vacuum conditions' (Arifov 1969). Under ultrahigh-vacuum conditions the influence of adsorbed particles can indeed be neglected but the role of impurities deposited by the ion beam is still important. As was shown firstly by Snoek *et al* (1965), some structure in the energy spectrum of secondary electrons can be explained by Auger electron transitions inside a projectile previously embedded in the target material. Structure in the low-energy range of the spectrum may also appear owing to decay of atomic and molecular auto-ionisation states. A helium auto-ionisation peak from the metal surface saturated by helium projectiles was observed by Soszka (1972). A broad peak was reported to be the result of molecular auto-ionisation for violent collisions between the bombarding ions and previously embedded ions by Budzioch *et al* (1986). However, the structure men-

0953-8984/89/071353 + 11 $02.50

tioned above is unstable with respect to time because of migration and sputtering of the embedded particles.

In this paper, we report an investigation of the yield of electrons from a cold metal target covered by condensed xenon under xenon ion bombardment.

2. Experimental conditions

The Fe–Ni alloy target was mounted on the cold finger of a flow cryostat. The cold finger was introduced into the vacuum chamber which had a residual gas pressure of about 5×10^{-10} Torr. Using a leak valve, it was possible to change the xenon gas pressure inside the chamber up to 10^{-6} Torr. Before measurements were taken, the nitrogen trap and then the target was cooled. The target was kept at liquid-nitrogen temperature (85 K) while the experiment was carried out. The xenon or neon single-energy ions impact the target surface perpendicularly ($\Psi = 90°$ where Ψ is the incidence angle; see the inset in figure 2). The ion current was measured with a movable Faraday cup and was about 15 nA during each measurement of the electron energy spectra and about 30 nA during the ion spectra measurements. The measured section consisted of a rotatable electrostatic energy analyser and a channeltron detector. The influence of a stray magnetic field on the slowly moving electrons was suppressed by accelerating the electrons prior to their entering the electrostatic analyser. The entrance of the channeltron was kept under an accelerating voltage which was higher than the energy of electrons. The energy resolution of the energy analyser was better than 1%, and the angular resolution was $\pm 0.2°$. The special computer equipment allows us to measure the energy spectra of electrons or energy spectra of back-scattered ions.

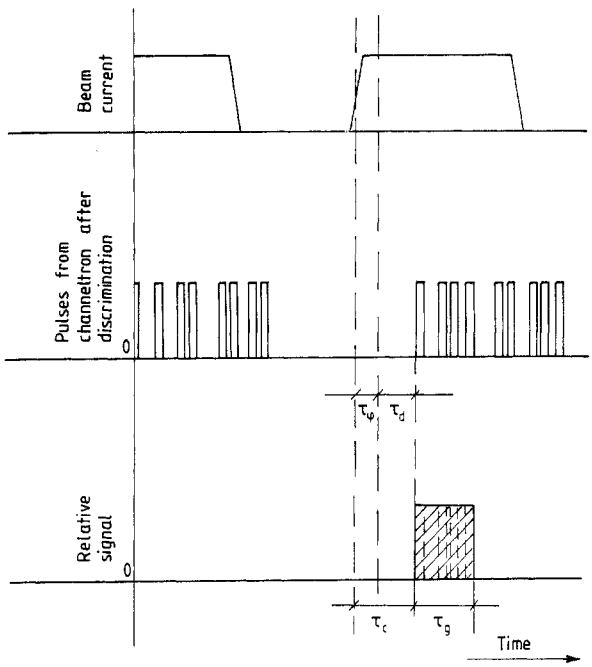

Figure 1. Time dependences in the coincidence-recording method of secondary particles with different masses.

It has been predicted that in work with metal targets covered by condensed gases a low-energy fraction of negative ions can be created and the electron energy data would be falsified. The negative ions were excluded using a coincidence-recording method based on the idea of the time of flight of particles with different masses inside the electrostatic analyser. The time dependences in this method are presented in figure 1. The electric chopper produced beam pulses which after a time τ_φ reached the target. The charged particles were recorded with a (channeltron) detector after a time $\tau_\varphi + \tau_d$ where τ_d is the time of flight of particle from target to detector through the energy analyser. The relative signal width τ_g (the coincidence time) and delay τ_c were chosen in such a way that during measurements on particles with the highest energy the negative ions could not reach the detector in a time equal to or shorter than $\tau_g + \tau_c$. This technique allowed us to distinguish between the secondary electrons and secondary negative ions (with the same kinetic energy) in the full range of measured energy.

Before the target was mounted in the vacuum chamber, its surface was mechanically polished and then the inside of the chamber was cleaned by argon sputtering.

3. Results

In figure 2 the energy spectra of secondary electrons induced by xenon ion bombardment of the Fe–Ni alloy target cooled to the liquid-nitrogen temperature (85 K) and kept in a

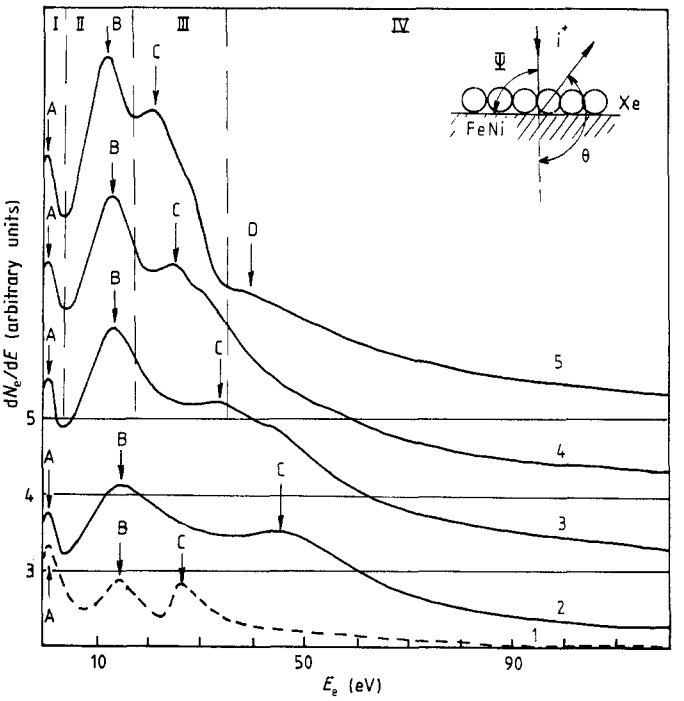

Figure 2. Energy spectra of secondary electrons induced by xenon ion bombardment of the Fe–Ni alloy target at the liquid-nitrogen temperature and in a xenon atmosphere with a pressure of 10^{-6} Torr (——) for various detection angles θ_e: curve 2, $\theta_e = 128°$; curve 3, $\theta_e = 136°$; curve 4, $\theta_e = 146°$; curve 5, $\theta_e = 156°$. The energy spectrum at a xenon pressure of 10^{-8} Torr and at a detection angle θ_e of 156° is also shown (curve 1, – – –). The primary-ion energy E_0 was fixed at 10 keV. The inset is a schematic illustration of the geometrical arrangement of the target.

xenon atmosphere with a pressure of 10^{-6} Torr are shown. The energy spectra were measured at different detection angles θ_e with a fixed incidence angle Ψ of 90° and at a primary-ion energy E_0 of 10 keV. The electron spectrum obtained at a xenon pressure of 10^{-8} Torr (broken curve) is also presented. Independent of a maximum which is typical of electron emission from the clean target (labelled A), two additional maxima B and C appear owing to xenon exposure. These maxima sharply increase with increase in the xenon pressure and become a dominant feature of the energy spectra. Analysis of the dependence on the detection angle θ_e shows that the intensity of peaks B and C increases with increase in θ_e, but peak B very slightly shifts and peak C much more significantly moves to lower energies with increase in θ_e. To simplify the explanation of the origin of the electrons, the energy spectrum has been divided into four parts: I, II, III and IV. In each part the electron yield reaches a local maximum: A in region I, B in region II, C in region III and D in region IV.

In figure 3 the electron spectra for three values of the primary-ion energy E_0 are presented. The other experimental parameters are the same as in figure 1. At small ion energies, only maximum B is observed and its intensity increases with increase in E_0.

In figure 4 the energy spectra of neon ions reflected by the cold Fe–Ni target at different xenon pressures inside the vacuum chamber are shown. At a xenon pressure of 10^{-8} Torr (full curve) the single-scattering peak for iron and less defined peak for nickel are observed. The peak connected with scattering of neon ions by xenon atoms is

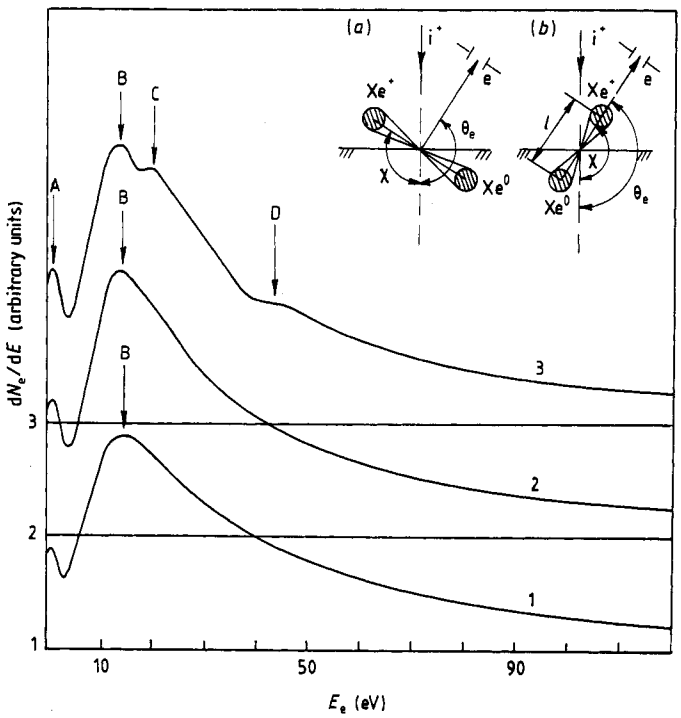

Figure 3. Energy spectra of secondary electrons for three values of the primary-ion energy E_0 (curve 1, E_0 = 6 keV; curve 2, E_0 = 8 keV; curve 3, E_0 = 10 keV) and at a fixed detection angle θ_e of 156°. Insets (*a*) and (*b*) are illustrations of the position of the quasi-molecule $Xe^+ + Xe^0$ during direct ionisation and during decay of the molecular auto-ionisation states, respectively.

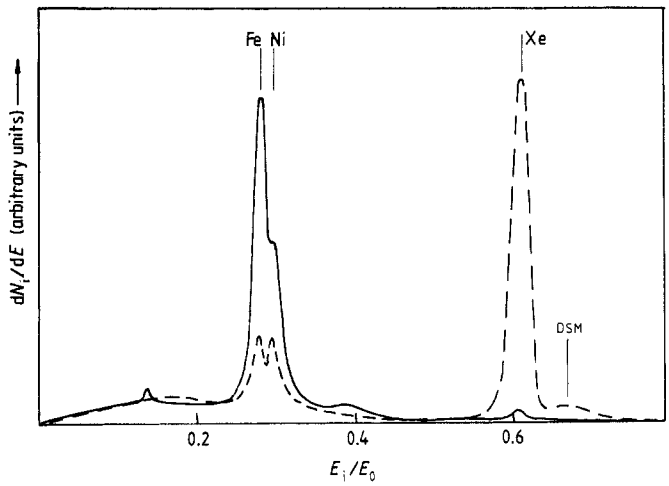

Figure 4. Energy spectra of 6 keV neon ions reflected by the cold (85 K) Fe–Ni target in a xenon atmosphere: ——, $p_{Xe} = 10^{-8}$ Torr; – – –, $p_{Xe} = 10^{-6}$ Torr; DSM, double-scattering maximum. The incidence angle Ψ and scattering angle θ_0 were 90° and 126°, respectively.

small but its intensity sharply increases with increase in xenon pressure (broken curve). In the range of higher energies the so-called double-scattering maximum which is attributed to the condensed state of xenon appears (Mashkova and Molchanov 1985). As the iron and nickel peaks can still be seen the xenon condensed layer is assumed to be relatively thin.

4. Discussion

The results show that the electron energy spectrum for a metal target covered by condensed xenon differs from the typical energy spectrum for a clean target (Benazeth 1982). The energy distribution of secondary electrons obtained consists of a continuous spectrum on which a few broad maxima are superimposed. The continuous spectrum ranges from zero to a few hundred electron volts and its shape is similar to those for gaseous targets (Woerlee *et al* 1981). If the results of analysis of reflected ions (the pronounced single-scattering peak of ions) are also taken into account, the following assumptions can be made.

(i) The 'one-collision' model can be used.

(ii) During collision, $Xe^+ + Xe^0$ quasi-molecules are created and their role as a source of secondary electrons is dominant.

There are a few models which can explain the origin of the continuous spectrum for gas targets (Woerlee *et al* 1981). One of these is the model developed by Russek and Thomas (1958) and Firsov (1959) which assumes that the yield of electrons from quasi-molecules is due to the kinetic energy of projectiles. The yield of electrons is proportional to the inelastic energy losses which are equal to the work of retardation forces in the interaction of electron clouds of ions and atoms. If the energy loss exceeds the energy of ionisation, an electron can leave a quasi-molecule by direct ionisation. When the evenly distributed electron density inside an atom is taken into account, it is possible to

calculate the electronic stopping cross section S_e (Lindhard and Scharff 1961) and from this the average inelastic energy losses Q as a function of impact parameter p and kinetic energy E_0 in the elementary interaction event (Oen and Robinson 1976).

Now we compare the maximum energy in the energy composition of secondary electrons (the high-energy cut-off of the energy distribution curve (figure 5)) with the inelastic energy losses Q of ions described by the formula of Oen and Robinson (1976). The electron with the maximum energy recorded under the defined experimental conditions (angle of detection and primary-ion energy) originates certainly from the violent collision between xenon ions and surface xenon atoms. In figure 6 the simulated position of the $Xe^+ + Xe^0$ quasi-molecule during each time interval $\Delta t = 2 \times 10^{-17}$ s is presented. The calculations were performed for the statistical Thomas–Fermi potential (Torrens 1972) with the Moliére (1947) approximation. The screening length was the same as in the Firsov (1957) formula. It can be seen that for a primary-ion energy E_0 of 10 keV and for an impact parameter p of 0.25 Å the electrons which are ejected perpendicular to the long axis of the quasi-molecule at the moment of closest approach will be recorded at a detection angle $\theta_{e\perp}$ of 128° and the electrons which are ejected parallel to the quasi-molecule at a detection angle $\theta_{e\parallel}$ of 142° (here $\theta_{e\perp} = \frac{3}{2}\pi - \theta_{e\parallel}$). So, when electrons are emitted perpendicular or parallel, for a fixed value of the detection angle θ_e of 128° the distance r_0 of closest approach was found as a function of E_0 and then the inelastic energy losses $Q_\perp$ and $Q_\parallel$ were calculated using the Oen–Robinson formula. The results of calculations are shown in figure 7. The inelastic energy losses $Q_\perp$ and $Q_\parallel$ increase linearly with increase in the incident-ion energy E_0. In the same figure the experimental dependence of the high-energy cut-off $E_1(E_0)$ of the energy distribution curve dN_e/dE (figure 5) as a function of E_0 is presented. Since the behaviours of the curves $Q(E_0)$ and $E_1(E_0)$ are similar, it can be concluded that the kientic mechanism of electron emission satisfactorily describes the origin of electrons with a higher energy (the tail of the continuous spectrum–part IV in figure 2).

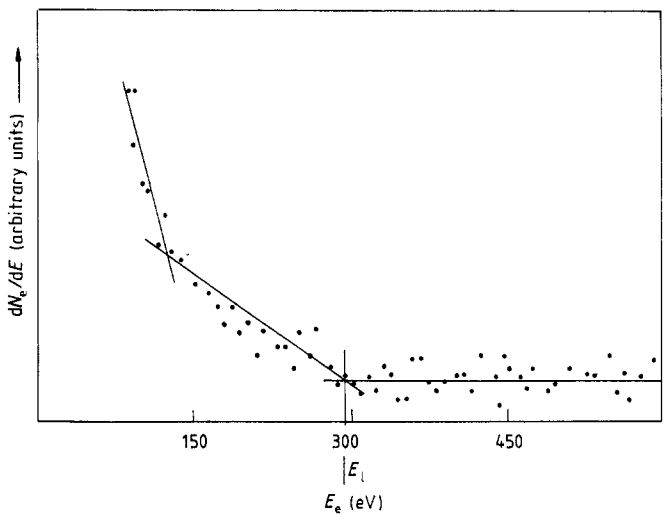

Figure 5. End of the energy distribution curve of secondary electrons at a large magnification (figure 2, curve 2). This illustrates the method of determination of the high-energy cut-off E_1.

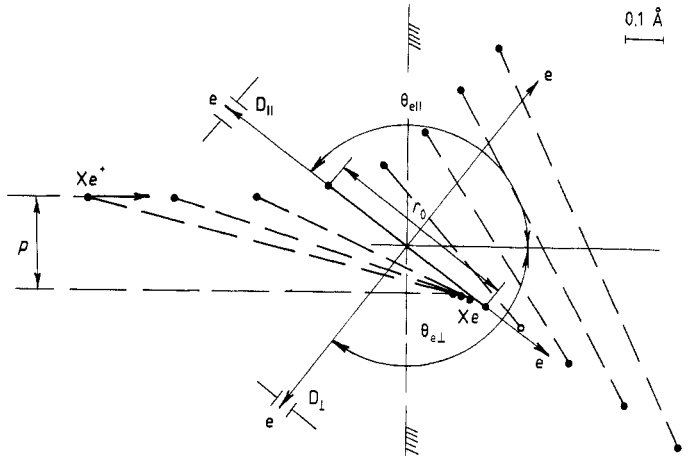

Figure 6. Simulated position of the $Xe^- + Xe^0$ quasi-molecule in the laboratory system during each time interval Δt of 2×10^{-17} s at an incident ion energy E_0 of 10 keV and an impact parameter p of 0.25 Å.

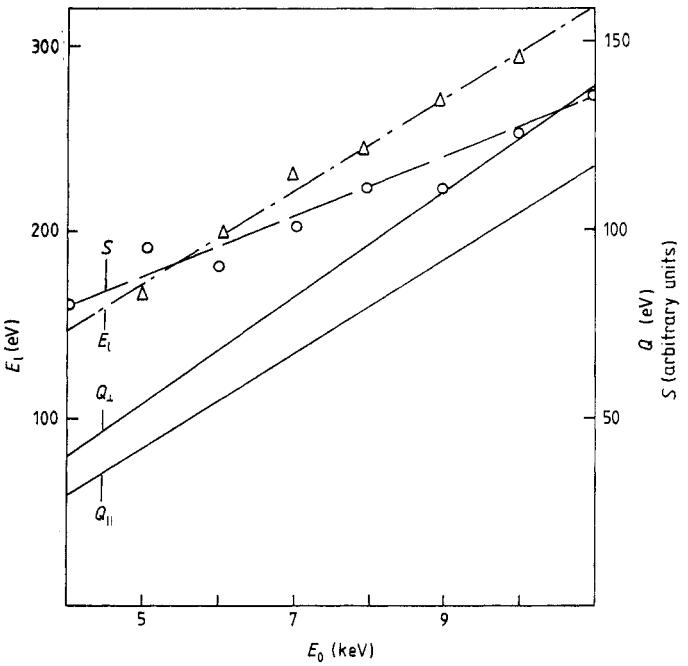

Figure 7. Calculation results: dependence of the average energy inelastic losses $Q_{\perp}$ and $Q_{\parallel}$ on the primary-ion energy E_0; △, ———, experimental dependence of the high-energy cut-off E_i of the energy distribution curve dN_e/dE on the primary-ion energy E_0; ○, ——, experimental dependence of the total area S under the energy distribution curve from figure 2 on the primary-ion energy E_0. The detection angle θ_e was 128°.

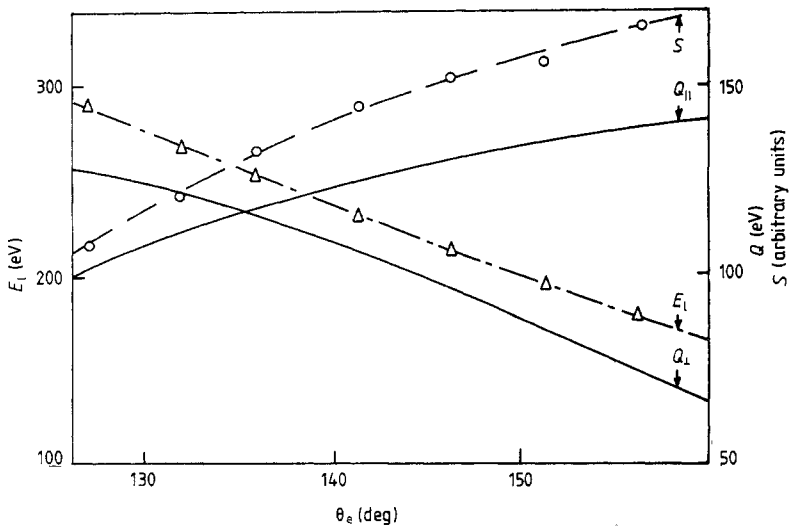

Figure 8. The same dependences as in figure 7 but on the detection angle θ_e and at a fixed primary-ion energy E_0 of 10 keV.

In figure 8 the average inelastic energy losses $Q_{\perp}(\theta_e)$ and $Q_{\parallel}(\theta_e)$ and the high-energy cut-off of the energy distribution curve $E_l(\theta_e)$ as a function of the detection angle θ_e are compared. The maximum energy of the electrons decreases with increase in the detection angle at fixed incident ion energy. Similar behaviour is observed for the $Q_{\perp}(\theta_e)$ curve. This means that electrons are emitted from the quasi-molecule perpendicular to its long axis. We think that the process of direct ionisation takes place during the approach of colliding particles; thus the electrons, which arise mainly from the deeper-lying atomic shells, are 'pushed' in the direction perpendicular to the long axis of the quasi-molecule.

Some electrons will be excited and they can occupy the optical levels near the continuum. If one electron from the inner shell or two or more electrons from the outer shell are excited, the excitation energy exceeds the first ionisation limit and such a state is known as an auto-ionisation state. Since the auto-ionisation time τ_a is relatively short (Ogurtzov 1972), auto-ionisation decay can take place during the existence of the quasi-molecule (molecular auto-ionisation) and while the collision particles recede. Owing to the reconstruction of the electronic system an electron leaves the quasi-molecule with a kinetic energy E_k^i:

$$E_k^i \simeq (E_v - \Delta E_1) - (E_{1i} - \Delta E_2) \tag{1}$$

where the superscript i indicates the inner-shell auto-ionisation process, E_v is the binding energy of electron in the subshell v in which the initial vacancy is created during previous direct ionisation or excitation, E_{1i} is the first ionisation limit, and ΔE_1 and ΔE_2 are energy corrections due to a change in the potential energy according to the correlation diagrams of interaction (Barat and Lichten 1972). Theoretical calculations show (Ogurtzov 1972) that the Auger transition probabilities (the inner-shell auto-ionisation processes can be treated as a type of Auger process) are from 10^{12} to 10^{15} s^{-1} or that the time τ of Auger transitions varies from 10^{-15} to 10^{-12} s. If the vacancy is created at the moment of closest approach, then, because of finite time τ, the inner-shell auto-ionisation decays are realised at the inter-nuclear separation l and at the moment when the collision

partners recede. Generally, the quasi-molecule rotates during interaction (see figure 6) and the distance l is not parallel to the distance r_0 of closest approach. However, as a special simulation program shows (Robinson and Torrens 1974), the rotation of the quasi-molecule can be neglected in violent collisions and then the inter-nuclear separation l is a function of r_0 and τ:

$$l = r_0 + \tau v_0 \tag{2}$$

where v_0 is the incident ion velocity.

It is also possible that two or more electrons will be excited from the outer shell. The kinetic energy of electrons which are liberated in the outer-shell auto-ionisation processes E_k^o can be estimated from the following formula:

$$E_k^o \simeq (E_{2i} - \Delta E_3) - (E_{1i} - \Delta E_4) \tag{3}$$

where the superscript o indicates the outer-shell auto-ionisation process, E_{1i} and E_{2i} are the ionisation limits, and ΔE_3 and ΔE_4 are the corrections due to interactions. The differences $\Delta E_1 - \Delta E_2$ and $\Delta E_3 - \Delta E_4$ determine the kinetic energy of electrons from the inner-shell and outer-shell auto-ionisation processes and they are a function of the inter-nuclear separation l.

The analysis of the correlation diagrams shows (Barat and Lichten 1972) that the first difference (inner-shell excitation) depends on l more strongly than does the second difference (outer-shell excitation). This means that the kinetic energies of electrons originating from the auto-ionisation decay of the quasi-molecules with different dimensions should evidently change for inner-shell auto-ionisation. For outer-shell auto-ionisation processes the kinetic energies should change weakly. The preferred outlet of electrons with a discrete energy (Budzioch *et al* 1986) means that, at a fixed detection angle, only quasi-molecules with defined dimensions should participate in the auto-ionisation processes. The above discussion allows us to conclude the following.

(i) Peak C in figure 2 which distinctly shifts on the energy scale with change in the detection angle is connected with the molecular inner-shell auto-ionisation processes.

(ii) Peak B which is almost stable on the energy scale is connected with the molecular outer-shell auto-ionisation processes.

The identification of peaks based on the values of electron energy is difficult for electrons from quasi-molecular processes because the correlation diagrams are very complex.

In figures 7 and 8 the total area S under the energy distribution curve $\mathrm{d}N_e/\mathrm{d}E$ (figure 2) as a function of E_0 and θ_e are shown (S is proportional to the coefficient of the ion–electron emission). The total electron yield increases with increase in the incident-ion energy and detection angle and the behaviours of the $Q_{\|}(E_0)$ and $Q_{\|}(\theta_e)$ curves are similar. On the assumption that the kinetic mechanism is still responsible for the excitation energy, the results obtained suggest that the auto-ionisation electrons leave the quasi-molecule in a direction parallel to its long axis (Budzioch *et al* 1986). Moreover, the following considerations support the above suggestion. Excited electrons become common for systems of two particles, and the orbital velocities of the excited electrons are relatively high (the same order of magnitude as the Bohr velocity). Let the vacancy be connected with the core of the recoil atom. The probability of auto-ionisation decay reaches a maximum when the velocity v_e of the electron and the velocity v_v of movement of the vacancy are almost the same both in value and in direction. Because of the relatively high electron velocity, the condition mentioned above is fulfilled for violent

collisions and for the participation of high-energy projectiles. For such collisions the probability of auto-ionisation strongly increases and the electrons leave the quasi-molecule in a cone the axis of which is parallel to the long axis of the quasi-molecule.

Inner-shell auto-ionisation should markedly increase for light target particles because under the same experimental conditions the velocity v_v is larger than for the heavy target particles. This latter feature of auto-ionisation electron emission may be used in the angle-resolved ion–electron spectroscopy (ARIES) technique for identification of the surface impurities which, as a rule, are lighter than the substrate target particles (Soszka *et al* 1980).

Now we consider the intensities of peaks B and C (figures 2 and 3). The intensity of peak B increases with increase in incident-ion energy or with increase in the detection angle in the experimental range of E_0 and θ_e used. For peak C, some energetic threshold exists ($E_0 \simeq 9$ keV) and the peak intensity reaches a maximum at $\theta_e \simeq 136°$.

The total yield of auto-ionisation electrons is proportional to the cross section for collision, the cross section for inelastic energy transfer and the probability of auto-ionisation decay; see above. The number of collisions decreases with increase in the scattering angle θ_0 or with increase in the detection angle because $\theta_0 \simeq \frac{1}{2}\theta_{e\|}$. As the cross section for inelastic transfer (Firsov 1959) and the probability of auto-ionisation increase with increase in the detection angle, so an optimum angle of detection should exist for auto-ionisation emission. Indeed, peak C (figures 2 and 3) connected with inner-shell auto-ionisation reaches a maximum at a detection angle θ_e of about 136°. For inner-shell auto-ionisation processes the number of possible collisions which contribute to the yield of electrons is relatively small because the excitation energy is high. The electrons from the different violent collisions have different energies and this is why peak C is very broad (figure 2). For outer-shell auto-ionisation the number of collisions which contribute to the yield of the electrons is larger because the excitation energy is smaller. At small detection angles, only electrons from weak collisions contribute to the auto-ionisation yield. At large detection angles, in contrast with the inner-shell processes, the total auto-ionisation yield gives the well defined peak (peak B in figures 2 and 3) being the superposition of electrons from weak and violent collisions because the electron energy weakly depends on the quasi-molecule dimensions at the moment of decay. In the experiments a strong increase in the intensity of peak B with increase in the detection angle is observed. Such behaviour of peaks B and C is in the good agreement with the molecular auto-ionisation model.

Peak A in figures 1 and 2 is the maximum of the energy distribution of bulk electrons from the metal target which is superimposed on the background of electrons from the direct ionisation (the yield of these electrons reaches a maximum at $E_0 \simeq 0$ eV). This causes peak A to increase distinctly with increase in the concentration of the surface xenon particles (figure 2).

5. Conclusion

The energy spectra of secondary electrons emitted from a metal target covered by condensed xenon and from a clean cold target are completely different. For a metal target covered by compressed xenon and bombarded with xenon ions, symmetric quasi-molecules $Xe^+ + Xe^0$ can be created and their role in the ion–electron emission is dominant. It is seen in particular in the differential energetic and angular measurements. The electrons both from direct ionisation and from the decay of the molecular auto-

ionisation states leave the quasi-molecule in the defined direction relative to its long axis. If experiments are carried out with sufficient precision, the presence of the $Xe^+ + Xe^0$ quasi-molecules is manifested by structure in the energy spectrum and anisotropy in the ejection of the secondary electrons. On the basis of this, identification of the origin of the electrons is possible. The same effects should occur for a metal target at room temperature saturated by projectiles deposited by an ion beam although the process is unstable with respect to time.

Acknowledgment

This work was partially supported by Scientific Research Project CPBP 01.06.08.02.

References

Arifov U A 1969 *Interaction of Atomic Particles with a Solid Surface* (New York: Consultants Bureau)
Barat M and Lichten W 1972 *Phys. Rev.* A **6** 211
Benazeth N 1982 *Nucl. Instrum. Methods* **194** 405
Budzioch J, Soszka M and Soszka W 1986 *Nucl. Instrum. Methods* B **14** 530
Firsov O B 1957 *Zh. Eksp. Teor. Fiz.* **33** 696
—— 1959 *Zh. Eksp. Teor. Fiz.* **36** 1517
Krebs K H 1968 *Fortschr. Phys.* **16** 419
Lindhard J and Scharff M 1961 *Phys. Rev.* **124** 128
Mashkova E S and Molchanov V S 1985 *Medium-energy Ion Reflection from Solids* (Amsterdam: North-Holland)
Moliére G 1947 *Z. Naturforsch.* a **2** 133
Oen O S and Robinson M T 1976 *Nucl. Instrum. Methods* **132** 647
Ogurtsov G N 1972 *Rev. Mod. Phys.* **44** 1
Robinson M T and Torrens J M 1974 *Phys. Rev.* B **9** 5008
Russek A and Thomas M T 1958 *Phys. Rev.* **109** 2015
Snoek C, Gebelle R, Van der Weg W F, Rol P K and Bierman D J 1965 *Physica* **31** 1553
Soszka M and Soszka W 1983 *Acta Phys. Pol.* A **64** 255
Soszka W 1972 *Physica* **60** 257
Soszka W, Algra A J, Suurmeijer E P Th M and Boers A L 1980 *Radiat. Eff.* **51** 171
Torrens J M 1972 *Interatomic Potentials* (New York: Academic)
Woerlee P H, Gordeev Yu S, de Waard H and Saris F W 1981 *J. Phys. B: At. Mol. Phys.* **14** 527